Statistical Optimization and Modeling of Methylene Blue Adsorption Onto Graphene Oxide in Batch and Fixed-Bed Column

Habib Koulivand, Afsaneh Shahbazi*

Environmental Science Research Institute, Shahid Beheshti University, Tehran, Iran

*Correspondence to
Afsaneh Shahbazi,
Environmental Science
Research Institute, Shahid
Beheshti University, Tehran,
Iran.
Email: a_shahbazi@sbu.ac.ir

Abstract
The batch and fixed-bed column adsorption of methylene blue (MB), a widely used toxic dye, onto graphene oxide (GO) was investigated in this study. GO was synthesized using modified Hummers method and characterized by scanning electron microscopy (SEM), X-ray diffraction (XRD), and Fourier transform infrared spectroscopy (FTIR). Response surface methodology (RSM) was employed to optimize batch and fixed-bed column adsorption of MB. Batch adsorption experiments were carried out by central composite design (CCD) with three input parameters including initial MB concentration (C_0: 50-350 mg/L), GO dosage (D: 0.05-0.7 g/L), and pH (pH: 3-9). The adsorption capacity of GO for MB removal in the optimum level of factors (C_0: 50 mg/L, D: 0.05 g/L, and pH: 8.5) was predicted by the model to be 700 mg/g. Adsorption kinetic data were tested using pseudo-first order, pseudo-second order, and intraparticle diffusion models. The kinetic experimental data was well fitted with pseudo-second order kinetic model ($R^2=1$). The adsorption of MB onto GO demonstrated that Langmuir model ($R^2=0.999$) could better fit the adsorption data than the Freundlich model ($R^2=0.914$). Thermodynamic parameters including enthalpy (ΔH), Gibbs free energy (ΔG), and entropy (ΔS) were also investigated. Positive value of ΔH and negative value of ΔG indicated the endothermic and spontaneous nature of the adsorption. The positive value of ΔS also showed increased randomness at the solid/liquid interface during the adsorption of MB onto GO. The real wastewater experiment at optimum conditions showed high performance of adsorbent in the presence of other ions. Fixed-bed column experiments were designed using a three-factor, three-level Box-Behnken design (BBD) to investigate the single and combined effects of influent concentration (C_{inf}: 50-200 mg/L), flow rate (Q: 0.25-0.8 mL/min), and bed height (BH: 3-7 cm). MB removal from GO in the optimum levels of factors (C_{inf}: 51 mg/L, BH: 5.7 cm, and Q: 0.25 mL/min) was predicted by the model to be 86% (q_e=459.3 mg/g). Fixed-bed experimental data were also fitted well to the Thomas and BDST models. The results showed that GO can be used as an efficient adsorbent for batch and fixed-bed adsorption of cationic dyes from synthetic and real wastewater.
Keywords: Methylene blue, Graphene oxide, Fixed-bed column, Optimization, Real wastewater

1. Introduction

The control of water pollution has become one of the significant environmental problems in recent years. Dyes are widely used and are present in wastewaters of many industries such as plastic, textile, dyestuff, paper, leather, and so on (1). More than 100 000 commercial dyes are known with an annual production of over 700 000 tons/year. Total consumption of dye simply for textile industry is more than 10 000 tons/year and about 100 tons/year of these dyes are discharged into water streams (1). The presence of even very low concentrations of dyes make it undesirable due to its appearance. Most of the organic dyes have aromatic rings in their structure which make them very toxic and non-biodegradable. Hence, removal of these dyes from industrial effluents before discharging into natural waters is very important. Methylene blue (MB), a toxic basic azo dye, ($(CH_3)_2N(C6H3)NS^+(C_6H3)N(CH3)_2Cl^-$), has very wide applications in printing calico, dying cotton, leather and wood, hair colorant, and so forth (2, 3), and can cause harmful effects such as eye burns, methemoglobinemia, cyanosis, convulsions, tachycardia, dyspnea, and irritation to the skin (2).

Among numerous methods, adsorption is one of the widely used techniques in the removal of pollutants from aquatic environments due to its flexibility, low cost, ease of operation, and high resistance to toxic chemical compounds in water (3). Carbon-based nanomaterials have been recognized as excellent adsorbents for their

potential environmental applications in removing the pollutants (4). Graphene oxide (GO), a monolayer or few layers (<10) of sp^2-bonded carbon atoms densely assigned to a two-dimensional (2D) honeycomb lattice is a reliable carbon based nano-sorbent which consists of a number of oxygen-containing functionalities such as carboxyl, epoxy, ketone, and hydroxyl groups that impart a negative charge density to it in aqueous solution at a wide range of pH values (5). Therefore, recently, great efforts have been made to explore the applications of GO in the removal and recovery of pollutants such as dyes (5,6), heavy metals (7,8), polycyclic aromatic hydrocarbons (9,10), and so on from the aqueous solutions and wastewater.

Most studies have been conducted on dye removal in batch adsorption system; however, fixed-bed column adsorption system has been rarely studied. Fixed-bed column (continues) adsorption is closer to the real wastewater treatment plants and there are limited studies focused on fixed-bed column adsorption of pollutants onto GO. In addition, conventional and classical methods of studying a process by maintaining other factors involved at an unspecified constant level do not depict the combined effect of all the factors involved. This method is also time consuming and requires large number of experiments to determine optimum levels, which are unreliable. These limitations of a classical method can be eliminated by optimizing all the affecting parameters collectively by statistical experimental design such as response surface methodology (RSM). RSM consists of a group of empirical techniques devoted to the evaluation of relationships existing between a cluster of controlled experimental factors and measured responses according to one or more selected criteria.

The present study aimed to study and optimize the batch and fixed-bed column adsorption of MB onto GO. To achieve this purpose, GO was synthesized, characterized, and used for batch and fixed-bed column adsorption of MB from the synthetic and real wastewater. The effect of factors such as pH, initial dye concentration, and adsorbent dosage in batch experiments were investigated and optimized. The effect of temperature was also studied at optimum conditions. Since the prediction of dynamic behavior of adsorption by fixed-bed column experiment is important for an optimal design of an industrial adsorption process, according to batch adsorption results and adsorption capacity of GO, fixed-bed column experiments were chosen to study the effects of column condition including bed height, initial concentration, and flow rate. Fixed-bed column experimental data were fitted to various kinetic models to predict the behavior of the system. Finally, performance of GO for the removal of MB from the real wastewater was investigated.

2. Methods
2.1. Materials
Methylene blue (MW:319.85 g/mol), graphite extra fine powder (~325 mesh, 99.9995%), sulfuric acid (H_2SO_4, 98%), hydrochloric acid (HCl, 37%), sodium hydroxide (NaOH), potassium persulphate ($K_2S_2O_8$), phosphorus pentoxide (P_2O_5), potassium permanganate (KMnO4), and hydrogen peroxide (H_2O_2) were purchased from Merck Company (Germany). Deionized (DI) water was used in all experiments.

2.2. Synthesis and Characterization of Graphene Oxide
GO was synthesized by oxidizing graphite powder using modified Hummer's method (11). First, graphite powder, K_2S_2O8, and P_2O_5 were placed on a reaction flask. Then, H_2SO_4 was added to the reaction flask and stirred at 80°C for 6 hours. After completing the reaction, the solution was diluted with DI water and the mixture was stirred overnight, filtered, washed with DI water, and then dried to get the powder form of graphite oxide. Next, sulfuric acid and KMnO4 were added to the filtered graphite oxide respectively and stirred for 4 hours at 35°C. Then, DI water was added to the solution in ice batch. After 1 hour, H_2O_2 was added to the reaction flask, and stirred at the room temperature. Then, the GO was filtered and washed with HCl (0.1 N) to remove metal ions and impurities, followed by a wash with DI water to remove the acid.

Scanning electron microscopy (SEM; LEO 1455VP, Cambridge, UK) at accelerating voltage of 30 kV was applied for the characterization of surface structure and morphology of GO. The X-ray diffraction (XRD) pattern was recorded on an XRD spectrometer (Philips-PW 17C diffractometer). The scan was performed over a range of 5-80º 2θ. The FTIR spectra were recorded using a Fourier transform infrared spectrometer (Shimadzu 4600 spectrometer) in the range of 500-4000 cm^{-1}. Raman spectra were measured using LABRAM HR (Jobin Yvon, Horiba) with excitation wavelength of 514.5 nm. The zeta potential of the GO was measured using a zeta-sizer (Nano ZS-90, Malvern).

2.3. Batch Adsorption Study
2.3.1. Batch Experimental Design and Optimization by RSM
All batch adsorption experiments were conducted in a flask containing 30 mL of MB solution with different initial concentrations and adsorbent dosage and shaken at 300 rpm using shaker incubator at 25±1°C. After each adsorption experiment, the adsorbent was separated using centrifugation and the concentration of MB was measured using spectrophotometer (Hach DR 2800) at λ_{max} of 662 nm. The adsorbed mass (mg/g) and removal percentage (%) were calculated using equations 1 and 2, respectively:

$$q_e = \frac{(C_0 - C_e)V}{W} \tag{1}$$

$$R\% = \frac{(C_0 - C_e)V}{C_0} \times 100 \qquad (2)$$

Where q_e is the equilibrium adsorption capacity of the GO in mg/g, C_0 is the initial concentration of MB in mg/L, C_e is the concentration at equilibrium of MB in mg/L, V is the volume of solution in L, and W is the weight of the GO in g.

The optimum conditions for maximizing the adsorption of MB by GO were determined by means of a 3-factor, 3-level central composite design (CCD) combined with RSM and quadratic programming. In the first step of RSM, a suitable approximation is introduced to find a true relationship between the dependent variable (response, qe mg/g) and the set of independent variables (factors, including pH, initial concentration, and adsorbent dosage). Each independent variable was consecutively coded as x1, x2, and x3 at 3 levels (−1, 0, and +1). The experimental range and levels of independent variables considered in this study are presented in Table 1. Generally, the CCD consists of 2^k factorial runs with 2k axial runs and x_0 center runs. The 3-factor, 3-level CCD leading to 18 sets of experiments, including 8 factorial points (2^k), 6 axial points (2k), and 4 replicates at the center point (x_0) are reported in Table 1.

The center points were used to determine the experimental error of the dada. The number of experimental runs can be calculated using equation 3 (12):

$$N = 2^k + 2k + x_0 \qquad (3)$$

Where N is the number of experimental runs, k is the number of independent factors, and x_0 is the number of central points (replicates). For developing the regression equation, the coded variables were coded according to the following equation (equation 4):

$$X = \frac{x - [x_{max} + x_{min}]/2}{[x_{max} - x_{min}]/2} \qquad (4)$$

where x is the actual variable, X is the coded variable, and x_{max} and x_{min} are the maximum and minimum values of the actual variable.

In the next step, the behavior of the system is explained by the following quadratic polynomial equation (equation 5):

$$y = \beta_\circ + \sum_{i=1}^{k} \beta_i X_i + \sum_{i=1}^{k} \beta_{ii} X_i^2 + \sum_{i=1}^{k}\sum_{j=1}^{k} \beta_{ij} X_i X_j + \varepsilon \quad (5)$$

Where Y is the process response or output (dependent variable), k is the number of the patterns, i and j are the index numbers for pattern, β_o is the free or offset term called intercept term, β_i is the linear coefficient, β_{ii} is the quadratic coefficient, β_{ij} is the interaction coefficient, X_i and X_j are the coded values of the independent process variables, and $\mathcal{E}$ is the residual error.

The adequacy of the proposed model was validated using the diagnostic checking test, that is, analysis of variance (ANOVA). The property of the fitted polynomial model is represented by the coefficient of determination (R^2), the value of which assures a measure of how variability in the observed response values can be clarified by experimental factors and their interactions. These analyses were performed using the Fisher's 'F' test and P value (probability). An alpha (α) level of 0.05 was considered to determine the statistical significance in all analyses. Results were more statistically assessed by other descriptive statistics such as coefficient of determination, adjusted coefficient of determination, sum of squares, mean sum of squares, and coefficient of variation. The interaction among the different independent variables and their corresponding effect on the response was also studied by analyzing the response surface 3D plots.

2.3.2. Batch Adsorption Modeling
2.3.2.1. Kinetic Study

Sorption kinetics was studied in a 500 mL flask with 250 mL of MB solution (200 mg/L) at solution pH of 9, adsorbent dosage of 0.38 g/L, and room temperature of 25 ± 1°C. The samples were collected from solution flask at certain times (1-180 min) and the concentration of MB was measured. Different adsorption kinetic models including pseudo-first order, pseudo-second order, and intraparticle diffusion models were used to explain the adsorption kinetics.

The linear form of pseudo-first order (13), pseudo-second order (14), and intraparticle diffusion model (15) can be presented as 3quations 6, 7, and 8, respectively:

$$\log(q_e - q_t) = \log(q_e) - \frac{k_1}{2.303}t \qquad (6)$$

Where q_e and q_t are the adsorption capacity at equilibrium and at time t, respectively (mg/g), and k_1 is the rate constant of pseudo-first order adsorption (L/min). Values of k_1 and qe can be calculated from the slope and intercept of the plot of log (q_e – q_t) versus t.

$$\frac{t}{q_1} = \frac{1}{k_2 q_e^2} + \frac{1}{q_e}t \qquad (7)$$

Where k_2 (g/mg/ min) is the second-order rate constant of adsorption. Values of k_2 and q_e can be calculated from the intercept and slope of the plot of t/q_t versus t, respectively.

$$qi = k_i t^{0.5} + C \qquad (8)$$

Where k_i is the intraparticle diffusion rate constant (mg/g min$^{-0.5}$) and the intercept C, obtained by extrapolation of the plot of q_i versus $t^{0.5}$, back to the axis is taken to be proportional to the extent of the boundary layer thickness.

2.3.2.2. Isotherm Study

Equilibrium data, commonly known as adsorption isotherms, are basic requirements for the design of adsorption systems as they predict the adsorption capacity of adsorbent. In order to investigate the dye adsorption isotherm, Langmuir and Freundlich were fitted to the experimental adsorption data.

The linear form of Langmuir (16), and Freundlich (17) isotherm models can be written as Equations 9 and 10, respectively:

$$\frac{C_e}{q_e} = \frac{1}{K_a Q_m} + \frac{1}{Q_m} \times C_e \tag{9}$$

Where C_e (mg/L) is the equilibrium concentration of dye, and Q_m (mg/g) is the maximum adsorption capacity when the surface of adsorbent is completely covered with monolayer of adsorbate. K_a is adsorption equilibrium constant (L/g) which is related to affinity of binding sites or bonding energy of sorption. A plot of q_e/C_e versus q_e should represent a straight line with a slope of K_a and an intercept of $1/K_a Q_m$:

$$log q_e = log K_f \frac{1}{nf} log C_e \tag{10}$$

Where K_F is the Freundlich constant (L/g) related to the bonding energy coefficient and represents the quantity of dye adsorbed onto the adsorbent for unit equilibrium concentration. $1/n_F$ is the heterogeneity factor and n_F is a measure of the deviation from linearity of adsorption. Favorable range of $1/n_F$ is between 0 and 1. The plot of log (q_e) versus log (C_e) was employed to generate the intercept value of K_F and the slope of $1/n_F$.

2.3.2.3. Thermodynamic Study

Investigation of temperature effect on dye adsorption and determination of thermodynamic parameters of adsorption were performed at initial concentration of 200 mg/L, solution pH of 9, and adsorbent dosage of 0.38 g/L. The adsorption experiments were carried out for two hours at 10, 20, 30, 40 and 50°C.

The thermodynamic parameters, such as the Gibb's free energy (ΔG, kJ/mol), enthalpy (ΔH, kJ/mol), and entropy (ΔS, J/mol.K) changes associated with adsorption were determined using the Gibb's free energy (equation 11) and van't Hoff (equation 12) equations (18):

$$ln\, K_c = \frac{\Delta S}{R} - \frac{\Delta H}{RT} \tag{11}$$

$$\Delta G = \Delta H - T\Delta S \tag{12}$$

Where K_C is the distribution coefficient of adsorption, R is the universal gas constant (8.314 J/ mol.K), and T is the adsorption temperature (K). The values of ΔH and ΔS were calculated from the slope and intercept of the van't Hoff plot (ln K_C versus 1/T).

2.3.3. Real Wastewater Experiment

The performance of GO in the removal of MB from textile wastewater was also investigated. The real wastewater was provided from the Acryltab textile factory in Noshahr, Iran. The sample was collected and held in a cooled glass bottle with an ice bag and transported to the laboratory for analysis. Concentrations of different elements (such as Na, K, Mg, S, Si, Fe, and Zn) were measured in the collected sample. Then, MB was added to the sample and placed in a reaction flask to investigate the MB removal by GO from real textile wastewater at optimum conditions resulted from batch experiments.

2.3.4. Desorption and Regeneration Study

The mixture of 2% NaOH aqueous solution and ethanol (1:1, v/v) was employed as regeneration agent to recover the MB-loaded GO. Desorption experiments were performed at the optimum conditions resulted from batch experiments. The regenerated adsorbents were collected by filtration from the solutions, washed with distilled water, and then reused in the next cycle of adsorption experiments. The adsorption–desorption experiments were conducted for 5 cycles. All the experiments were performed at room temperature.

2.4. Fixed-Bed Column Adsorption Study
2.4.1. Fixed-Bed Column Experimental Design and Optimization by RSM

Continuous adsorption experiments were conducted in a glass column (6 mm internal diameter and 35 cm height). For the preparation of column, sand with grain size of 0.5–0.6 mm was washed with tap water, 10% nitric acid (v:v), and deionized water, respectively, then dried at 70°C, following the procedure of Ding et al (19) to remove loose impurities and metal oxides. The column was filled with 1% (w/w) GO/sand mixture, forming a homogenous and well-packed bed. The bed was supported and closed by glass wool, which ensured a good liquid distribution.

To investigate the performance of fixed-bed column system, a 3-factor, 3-level Box–Behnken design (BBD) combined with response surface modeling (RSM) and quadratic programming was applied. Known concentrations of MB (50, 125, and 200 mg/L) solution at pH of 6 and room temperature of 25±1°C was pumped upward through the adsorption column at different column bed heights (3, 5, and 7 cm) and solution flow rates (0.25, 0.52, and 0.80 mL/min), controlled by a peristaltic pump. The low, middle, and high levels of each variable were coded as -1, 0, and +1, respectively.

The number of experiments (N) required for the development of BBD is defined as N=2k(k−1)+CP, where k is the number of factors and CP is the number of central points. As seen in Table 2, a total of 17 column experiments were developed by BBD for the adsorption of MB. The MB solution at the outlet of the adsorption column (C_{eff}) was collected at certain time intervals and

its concentration was measured.

Dye removal efficiency by the column can be determined using the breakthrough curves obtained by plotting the dimensionless concentration (C_{eff}/C_{inf}) versus time profile, where C_{eff} and C_{inf} are the outlet and inlet adsorbate concentrations, respectively. The upper area in the breakthrough curve represents the total mass of adsorbed dye (q_{total}, mg) (20), which can be determined by the following equation (equation 13):

$$q_{total} = \frac{Q}{1000} \int_{t=0}^{t=t_{total}} (C_{ads}) dt \qquad (13)$$

Where C_{ads} is the concentration of dye adsorbed (mg/L), and Q is the flow rate (mL/min) and can be calculated as follows (equation 14):

$$Q = \frac{V_{eff}}{t_{total}} \qquad (14)$$

where V_{eff} (mL) is the effluent volume and t_{total} (min) is the total time. The total amount of dye sent to the column (mg) can be calculated using equation 15:

$$m_{total} = \frac{C_{inf} \times Q \times t_e}{1000} \qquad (15)$$

The MB removal percentage by column ($R\%$) can be calculated using equation 16:

$$R\% = \frac{q_{total}}{m_{total}} \times 100 \qquad (16)$$

The equilibrium adsorption capacity (q_e (mg/g)) can be calculated as follows (equation 17):

$$q_e = \frac{q_{total}}{m} \qquad (17)$$

Where m is the mass of GO (g).

A multiple regression modeling and graphical analyses of the experimental data were carried out using Design-Expert software for the analysis of the individual and combined effects of the independent test variables on the response (MB removal percentage). The significance of independent variables and their interactions were tested by means of the analysis of variance (ANOVA).

2.4.2. Fixed-Bed Column Adsorption Modeling
2.4.2.1. Thomas Kinetic Model

Thomas kinetic model was applied to the experimental data to predict the breakthrough curves and determine the characteristic parameters of adsorption for process design and scale up. The choice of the model was based on model assumptions. The model postulates that the sorption process follows the Langmuir isotherm and pseudo-second order kinetics while it is controlled by mass transfer at the interphase rather than the chemical reaction between the adsorbent and adsorbate (21, 22).

The expression of Thomas model for an adsorption column is given as follows (equation 18):

$$\frac{C_{eff}}{C_0} = \frac{1}{1 + exp(k_{Th} q_{Th} w / FR - k_{Th} C_0 t)} \qquad (18)$$

Where, k_{Th} is Thomas rate constant (mL /mg.min), q_{Th} is the equilibrium MB adsorption per gram of GO (mg/g), w is the mass of GO in the column (g), C_0 is the influent MB concentration (mg/L), C_{eff} is the effluent concentration at time t (mg/L), and FR is the flow rate (mL/min).

2.4.2.2. Adams–Bohart Model

The Adams-Bohart model also called bed depth service time model (BDST) was applied to fit the experimental data in order to determine the maximum sorption capacities and predict the bed service time and critical sorption depth (Z_0) at varying initial MB concentrations. This model assumes that the adsorption rate is proportional to both the residual capacity of the adsorbent and the concentration of the adsorbing species. In the fixed-bed systems, the main design criterion is to predict how long the adsorbent material will be able to sustain removing a specified amount of impurity from the solution before regeneration is needed. This period of time is called the service time (or break time) of the bed. BDST is a simple model for determining the maximum bed sorption capacity at different bed heights by establishing a linear relationship between bed height (H_b) and service time (t) by the following equation (equation 19) (23):

$$t = \frac{N_0 Z}{C_0 u} - \frac{1}{k_a C_0} \ln\left(\frac{C_0}{C_b} - 1\right) \qquad (19)$$

Where C_o is the influent MB concentration (mg/L), C_b is the breakthrough MB concentration (mg/L), N_0 is the sorption capacity of bed per unit bed volume (mg/L), u is the influent linear velocity (cm/min), k_a is the rate constant in BDST model (L/mg min), and t is the bed service time of column (min).

2.4.3. Estimation of Design Parameters for Column Scale Up

In order to scale up the lab-scale column, some factors that could characterize the mass transfer zone (MTZ) and its dynamics in relation to the changes in operational parameters were considered to guide future design. These factors include critical bed depth (Z_0), MTZ formation time (T_z), MTZ height (H_z), and MTZ velocity (U_z).

2.4.3.1. Critical Bed Depth (Z_0)

This value represents the sufficient height of the column in order to avoid breakthrough at t=0. The critical bed depths for 50, 125, and 200 mg/L influent concentrations were calculated based on the BDST model, using equation 20:

$$Z_0 = \frac{v}{K N_0} \ln\left(\frac{C_0}{C_b} - 1\right) \qquad (20)$$

2.4.3.2. MTZ Formation and Movement Time (T_z)

MTZ formation time is the time required for the formation and movement of MTZ along the bed depth of the column. This factor represents the rate of mass transfer and the bed length over which adsorption occurs within the column system. T_z can be calculated based on the flow rate (Q) and the volume of treated wastewater from the beginning until exhaustion (V_e) (equation 21) :

$$T_z = \frac{V_e}{Q} \qquad (21)$$

2.4.3.3. MTZ Height (H_z)

MTZ height is a parameter that indicates the portion of the column bed in which most of the mass transfer takes place. This parameter shows the removal rate of the pollutant by the adsorbent and can be used to calculate the overall adsorption kinetics within the system. The value of H_z can be calculated using equation 22:

$$H_z = \frac{H_b(t_s - t_b)}{t_b + f(t_s - t_b)} \qquad (22)$$

2.4.3.4. MTZ Velocity (U_z)

This factor directly refers to H_z and adsorption capacity and can be used to calculate the rate of bed saturation. It can be calculated using equation 23:

$$U_z = \frac{H_z}{(t_s - t_b)} = \frac{H_b}{(t_s - t_f)} \qquad (23)$$

Where H_z is the MTZ height (cm), H_b is the bed depth (cm), $t_f = 1-f$, and T_z is the time (min) required for the adsorption zone to form initially, while t_b and t_s are the times (min) at breakthrough ($C_t/C_0 = 0.1$) and bed saturation ($C_t/C_0 = 0.9$), respectively.

3. Results and Discussion
3.1. Characterization

The morphology of GO is characterized by SEM image in Fig. 1a. GO represented the sheet-like structure with the large thickness, smooth surface, and wrinkled edge (10). As shown in Fig. 1b, the XRD pattern shows the sharp peak at $2\theta = 10.24$ which is related to the 0 0 1 reflection and demonstrates that the oxygen containing groups were formed successfully in oxidation reaction of graphite. The peaks of graphite at $2\theta = 22.8°$, $44.8°$, and $55°$ also are not found in the X-ray pattern of GO (24,25). Absence of the natural graphite peak indicates that synthesized GO is free of unoxidized graphite. The FTIR result of prepared GO is shown in Fig. 1c. GO is a layered carbonaceous material with numerous oxygen-containing functional groups,
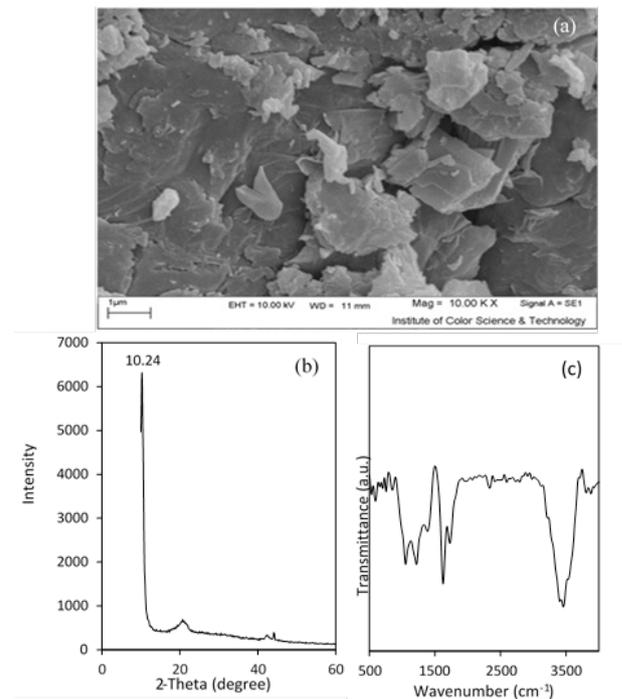
Fig. 1. (a) Scanning Electron Micrographs, (b) X-ray Diffraction Patterns, and (c) FTIR Reflectance Spectra of the Synthesized GO.

including hydroxyl, epoxy, and carboxylic acid. The broad peak at 3420 cm^{-1} is related to vibrational frequencies of –OH groups, the peaks at 1730 and 1620 cm^{-1} are related to stretching vibrations of C=O and C=C, respectively, and the peaks at 1370 and 1070 cm^{-1} indicate carboxyl (-O=C-OH) and epoxy (C-O) stretching vibration groups, respectively (5,10,24).

The Raman spectrum of GO is shown in Fig. 2a. The Raman spectrum of GO shows a G-band at ~1590 cm^{-1} and a D-band at ~1340 cm^{-1}. The G-band is associated with the vibration of sp^2 carbon atoms, and the D-band is related to the vibration of sp^3 defective or out-of-order graphitic carbon atoms (26). The results of zeta potential measurement for GO at different pH values are shown in Fig. 2b. Zeta potentials of GO decreased with increasing the pH value. The PZCs were estimated to be ca. pH 7. It was obvious that in different pH values, the surface of GO is positively charged. With an increased pH, the adsorption capacity of GO for MB molecules increased and the number of positive charges on GO decreased (27).

3.2. Batch Adsorption Study
3.2.1. Optimization of MB Adsorption in Batch System

The individual and interactive effects of independent variables on the adsorption of MB onto GO were investigated using CCD approach. The results of experiment runs are presented in Table 1. Polynomial regression modeling was performed between the response variable (adsorption capacity, q_e mg/g) and actual variable
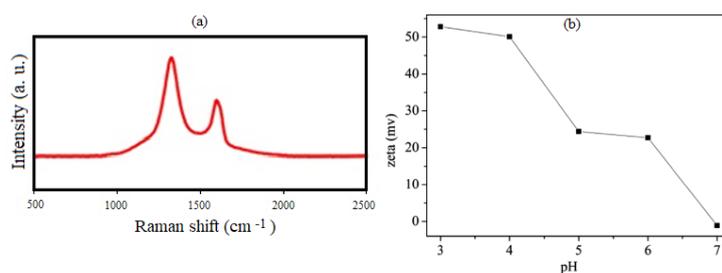
Fig. 2. (a) Raman Spectrum and (b) Zeta Potential of GO at Various pH Values.

(x_{pH}, x_{Co}, x_D) and the best fitted quadratic polynomial regression model was obtained as follows (equation 24):

$$q_e(mg/g) = 1.602\, x_{C_0} - 1927.048\, x_D - 35.184\, x_{pH} + 0.748\, x_{C_0} x_D + 0.018 x_{C_0} x_{pH} - 22.555\, x_D x_{pH} - 0.003\, x_{C_0}^2 + 1457.295 x_D^2 + 4.082 x_{pH}^2 + 719.952 \quad (24)$$

Adsorption capacity of GO in the optimum levels of factors (pH 8.5, initial concentration of 50 mg/L, and adsorbent dosage of 0.05 g/L) was predicted by the model to be 700 mg/g. Hameed et al could remove MB from aqueous solution with a maximum adsorption capacity of 454 mg/g using bamboo-based activated carbon (28). In another study, adsorption capacity of polydopamine microspheres for MB was 90.7 mg/g (4).

Analysis of variance (ANOVA) was employed to investigate the adequacy and significance of the model. According to the ANOVA results (Table 2), the value of F_{cal} was more than that of F_{tab} and P-value was lower than 0.05 which shows the significance and suitability of quadratic model. Moreover, the normal probability of the residuals almost indicated no departures from the normality (Fig. 3). High coefficient of determination (R^2=0.990) and adjusted coefficient of determination (R_{Adj}^2=0.979)

indicated the good agreement of experimental response values with model predicted values. The predicted R-squared was also in reasonable agreement with adjusted R-squared and showed a good prediction of model.

According to the batch experiments, the maximum adsorption capacity of the GO for MB removal was observed to be 940.0 mg/g (Table 2). The combined interaction between process parameters was described using 3-dimensional response surface plots.

Fig. 4a presents the interaction between pH and adsorbent dosage at a constant initial concentration (200 mg/L) of MB. According to Fig. 4a, by increasing the pH value from 3 to 9, the adsorption of MB onto GO was increased, and maximum adsorption was observed at pH 9. The pH of solution, as a significant factor of the adsorption process, influences the surface charge of adsorbent, degree of ionization of the material present in the solution, dissociation of functional groups on the active sites of adsorbent, and also the solution dye chemistry (29). At lower pH, the hydrogen ions compete with the dye molecules to get onto active sites on the surface of the adsorbent. Due to the occupation of the active sites of GO, the available sites for MB molecules

Table 1. Central Composite Design Matrix With 3 Independent Variables (Expressed Codes) and 2 Responses (q_e and R%) in Batch System

Runs	Batch conditions			Removal efficiency	
	Conc., mg/L (Coded Value)	Dose, g/L (Coded Value)	pH (Coded Value)	q_e (mg/g)	Removal Percentage (%)
1	50 (-1)	0.05 (-1)	3 (-1)	656.0	65.6
2	50 (-1)	0.05 (-1)	9 (1)	732.0	73.2
3	50 (-1)	0.38 (0)	6 (0)	132.5	99.4
4	50 (-1)	0.70 (1)	3 (-1)	71.0	99.4
5	50 (-1)	0.70 (1)	9 (1)	71.1	99.5
6	200 (0)	0.05 (-1)	6 (0)	740.0	18.5
7	200 (0)	0.38 (0)	3 (-1)	365.3	68.5
8	200 (0)	0.38 (0)	6 (0)	400.0	75.0
9	200 (0)	0.38 (0)	6 (0)	402.7	75.5
10	200 (0)	0.38 (0)	6 (0)	394.7	74.0
11	200 (0)	0.38 (0)	6 (0)	400.0	75.0
12	200 (0)	0.38 (0)	9 (1)	416.0	78.0
13	200 (0)	0.70 (1)	6 (0)	275.7	96.5
14	350 (1)	0.05 (-1)	3 (-1)	820.0	11.7
15	350 (1)	0.05 (-1)	9 (1)	940	13.4
16	350 (1)	0.38 (0)	6 (0)	453.3	48.6
17	350 (1)	0.70 (1)	3 (-1)	392.9	78.6
18	350 (1)	0.70 (1)	9 (1)	412.9	82.6

Table 2. Analysis of Variance for Response Surface Quadratic Model for the Prediction of Methylene Blue Removal Efficiency in Batch System

Source	Sum of Squares (SS)	df	Mean Squares (MSS)	F Value	Probability (P) > F	Significance
Model	1015000	9	112700	90.23	<0.0001	Significant
A-Concentration	184000	1	184000	147.25	<0.0001	Significant
B-Dosage	710000	1	710000	568.16	<0.0001	Significant
C-pH	7115	1	7115	5.69	0.044	Significant
AB	10632	1	10632	8.51	0.019	Significant
AC	511	1	511	0.41	0.540	
BC	3869	1	3869	03.10	0.117	
A^2	10082	1	10082	8.07	0.022	Significant
B^2	64202	1	64202	51.38	<0.0001	Significant
C^2	3657	1	3567	2.93	0.126	
Residual	9997	8	1250			
Lack of fit	9963	5	1993	176.97	0.7	
Pure error	2.5	3	0.83			
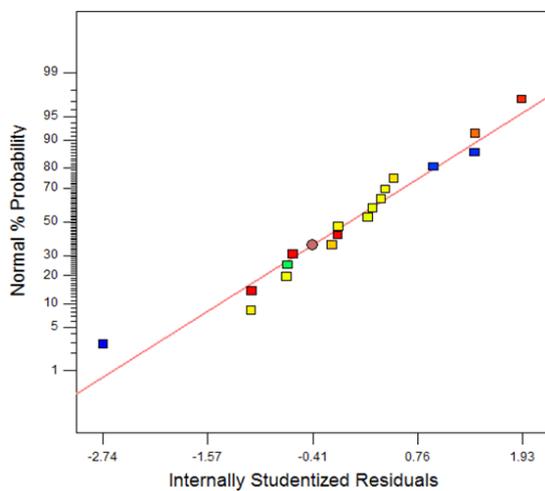
Fig. 3. Normal Probability of The Residuals in Batch Optimization.

Fig. 4. 3D Response Surface Plot of the Interactive Effects of (a) pH and Adsorbent Dosage, (b) Initial Concentration and Adsorbent Dosage, (c) Initial Concentration and pH, and (d) Percentage Of Contributions (PC%) for the Possible First-Order, Quadratic and Interaction Terms Onto Adsorption Capacity (q_e) in Batch System.

and also the adsorption capacity will be reduced. Quite the opposite, when pH increases, the GO surface has more negative charges, which can enhance the electrostatic interaction between the positively charged MB molecules and GO and higher uptake of dye molecules from water. Moreover, Fig. 4a shows that the adsorption capacity of GO increases by decreasing the adsorbent dosage. At the lower adsorbent dosages, almost all active sites are occupied while, at the higher adsorbent dosages, some of the active sites are not utilized by the MB molecules and this results in decreasing the adsorption capacity of adsorbent (30).

Fig. 4b shows the interactive effect of initial concentration and adsorbent dosage on the adsorption capacity (q_e mg/g) at a constant pH (6). There is a similar relationship between the adsorption capacity, dye concentration, and adsorbent dosage. As a rule, increasing the initial dye concentration provides a driving force to overcome all mass transfer resistance of dyes between the aqueous and solid phases, resulting in an increase in the adsorption

capacity (31). Hence, the maximum adsorption capacity of GO occurs at maximum value of initial concentration (350 mg/L) and at minimum value of adsorbent dosage (0.05 g/L). Fig. 4c presents the interaction between the pH and initial concentration at a constant adsorbent dosage (0.38 g/L). As shown in this figure, the maximum adsorption capacity of MB was obtained at the maximum values of pH (9) and initial concentration (350 mg/L). The percentage of contributions (PC%) for each individual term is calculated and presented in Fig. 4d, based on the sum of squares obtained from the ANOVA. According to the figure, the adsorbent dosage is the most significant term with a contribution of 71.4% as compared to the other components. Initial concentration of MB and pH of solution with contributions of 18.5% and 7.8%, respectively, are the other effective factors with lower importance. These values for the sum of interactions and

sum of quadratic effects were 1.5% and 0.72%, respectively.

3.2.2. Kinetic Study

The results of kinetic study are shown in Table 3. The kinetic studies showed that the adsorption of MB onto GO was approximately fast and about 50% of dye removal occurred in first 5 minutes and the sorption reached equilibrium within 2 hours. The correlation coefficient of kinetic data with pseudo-first order kinetic model was relatively high ($R^2 = 0.922$). It is also observed that the estimated equilibrium adsorption capacity value (28.9 mg/g) is much lower than the experimental value (344.7 mg/g). The results showed that the pseudo–second order can explain adsorption kinetics better than other kinetic models due to its noticeable high correlation coefficients ($R^2 = 1$) and agreeable prediction of q_e (344.8 mg/g). Pseudo-second order equation is based on the adsorption capacity (32). According to this model, occupancy rate of adsorption places is proportional to the square of the number of unoccupied places. Therefore, this equation can well describe the surface adsorption. Adsorption kinetics of MB onto bamboo-based activated carbon, published by Hameed et al, was also followed by pseudo-second order kinetic model (28). Whereas adsorption kinetics of MB onto commercial activated carbon was followed by pseudo-first order (33).

Intraparticle diffusion model was also employed to understand the rate limiting step of adsorption. High values of intercepts showed that the plot of q_i versus $t^{0.5}$ do not pass the origin. Therefore, intraparticle diffusion is not a rate limiting step and this limiting step is because of the occupation of active sites which confirm pseudo-second order kinetics. According to this model, adsorption includes 3 steps. The fast adsorption step ($k_i = 9.96$) at first 15 minutes was a result of more available active sites. The slow low adsorption step ($k_i = 1.77$) that occurred between 15 to 60 minutes, was because of the occupation of more active sites. The final step that was very slow ($k_i = 0.62$) was observed after 60 minutes to equilibrium time and saturation of active sites.

3.2.3. Isotherm Study

The isotherm constants for Langmuir ($K_a = 0.19$ g/L) and Freundlich ($K_f = 128.3$ g/L) were calculated (Table 4). The Langmuir model ($R^2 = 0.999$) exhibited better fits to the adsorption data than the Freundlich model ($R^2 = 0.914$) due to higher R^2 and infection and calculated Q_m value by Langmuir model (454.5 mg/g) which well agreed with the experimental data (453.3 mg/g).

The value of $1/n_F$ for Freundlich model (0.27) was between 0 and 1 which showed that adsorption of MB onto GO at experimental condition was favorable. Correlation of experimental data with the Langmuir model shows that the adsorption of MB onto GO is a monolayer process and can occur at an identical and finite number of sites (34). This model also confirmed the homogeneous nature

Table 3. Kinetic Model Constants for Adsorption of MB onto GO in Batch System

Model		Parameter	Value
Pseudo-first order		k_1 (1/min)	0.015
		q_e (mg/g)	28.86
		R^2	0.92
Pseudo-second order		k_2 (g/mg min)	142.68
		q_e (mg/g)	344.82
		R^2	1.0
Intraparticle diffusion	Step1	k_i (mg/g min$^{0.5}$)	9.96
		C	296.43
		R^2	0.98
	Step2	k_i (mg/g min$^{0.5}$)	1.77
		C	327.22
		R^2	0.96
	Step3	k_i (mg/g min$^{0.5}$)	0.62
		C	335.44
		R^2	0.78

Table 4. Isotherm Model Constants for Adsorption of MB Onto GO

Langmuir			Freundlich		
q_m (mg/g)	K_a (l/g)	R^2	$1/n_F$	K_F (l/g)	R^2
454.5	0.19	0.999	0.27	128.26	0.914

of adsorption, in which each molecule possesses constant enthalpies and sorption activation energy (35). The single layer and homogeneous structure of GO with the oxygen-containing functional groups justify this correlation. Isotherm result was in agreement with the adsorption of MB onto activated carbon (28) and presented monolayer adsorption of MB onto GO.

3.2.4. Thermodynamic Study

The values of ΔH and ΔS were calculated from the slope and intercept of the van't Hoff plot (Fig. 5). The endothermic nature of MB adsorption by GO was confirmed by the positive value of ΔH (14.95 kJ/mol). The increase of MB adsorption at higher temperature could be due to the increasing mobility of MB molecules, as well as the higher affinity of sites and increasing binding sites for MB molecules adsorption (36). The negative values of ΔG (-4.93, -5.64, -6.34, -7.04, -7.74) at all studied temperatures (283, 293, 303, 313, and 413 K, respectively) verified the thermodynamic feasibility and spontaneity of the adsorption process. The favorability of MB adsorption onto GO at higher temperatures was also revealed by the shifting of ΔG to more negative values with the increasing temperature. The positive ΔS value (0.07 kJ/mol K) suggests that the disorder at the solid−liquid interface increased during dye adsorption and also suggests that an increasing randomness occurs in solid/solution interface. The value of ΔG between -20 and 0, and also the value of ΔH between 8 and 25, both showed physical mechanism of adsorption.
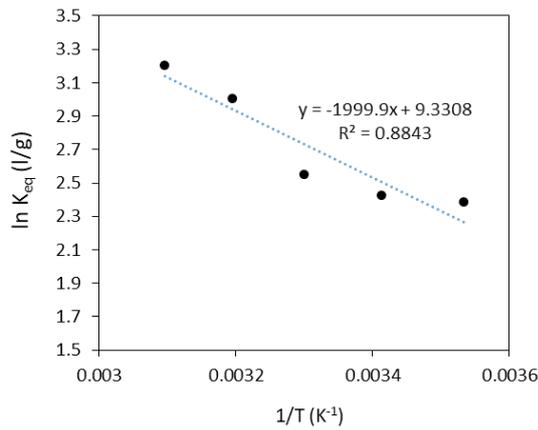
Fig. 5. Van 't Hoff Graph for Adsorption of MB Onto GO.

3.2.5. Real Wastewater Adsorption Experiment

It is well known that the textile wastewater does not contain only dye. To survey the performance of adsorbent for the removal of MB from the real wastewater, a batch experiment was conducted on textile wastewater. The result showed that the adsorbent gave a high performance in the removal of MB in presence of other contaminants. As in optimum conditions (pH of 6, initial concentration of 50 mg/L, and adsorbent dosage of 0.05 g/L), the removal percentages of MB by GO from synthetic and real wastewaters were respectively 68% and 65%. Na, S, Zn, and Fe were dominant ions in the real wastewater with the

concentrations of 396, 39, 29, and 3 mg/L, respectively. High performance of GO for MB adsorption in the presence of other ions can be described by the selective adsorption of MB molecules onto GO.

3.2.6. Desorption and Regeneration

Since the recycling and regeneration of adsorbent is very important in practical applications, the regeneration experiments for GO after saturated adsorption, which have relatively high MB uptakes, have been carried out. The results of GO desorption and regeneration are presented in Table 5. The adsorption and desorption processes were repeated to examine the potentials of GO. Table 5 shows that the recovery efficiency of GO is generally high and the adsorption capacity is little affected in 5 consecutive adsorption–desorption cycles. In all, due to the high recycling efficiency, this GO is qualified for practical application.

3.3. Fixed-Bed Column Adsorption Study
3.4.1. Optimization of MB Adsorption in Fixed-Bed Column System

The breakthrough curves (C_{eff}/C_o versus time) were obtained for the MB adsorption onto GO at different bed heights (BH: 3, 5, 7 cm) and various dye concentrations (C_0: 50, 125, 200 mg/L) at 3 influent flow rates (FR: 0.25, 0.52, 0.80 mL/min). The removal efficiency (qe and R%) in fixed-bed column system are summarized in Table 6.

The individual and interactive effects of independent variables on the adsorption of MB onto GO were investigated using BBD approach. Polynomial regression modeling was performed between the response variable

Table 5. Regeneration Efficiency of GO After Adsorption of MB

Cycle	1	2	3	4	5
Removal percentage (%)	68	61	56	52	47

Table 6. Box–Behnken Design Matrix With 3 Independent Variables (Expressed Codes) and 2 responses (q$_e$ and R%) and Thomas Model Constants for Fixed-Bed Column System

Runs	Column Conditions			Removal Efficiency		Thomas Model		
	Influent Concentration, mg/L (Coded Value)	Flow Rate (mL/min)	Bed Height (cm)	q$_e$ (mg/g)	R (%)	K$_{Th}$ (mL/mg min)	q$_{Th}$	R²
1	50 (-1)	0.25 (-1)	5 (0)	572.6	81.8	-	-	-
2	50 (-1)	0.52 (0)	3 (-1)	335.4	67.1	0.1341	347.3	0.9810
3	50 (-1)	0.52 (0)	5 (0)	374.9	67.0	0.1285	388.0	0.9986
4	50 (-1)	0.52 (0)	7 (1)	455.1	74.1	0.1017	501.4	0.9979
5	50 (-1)	0.80 (1)	5 (0)	354.6	65.7	-	-	-
6	125 (0)	0.25 (-1)	3 (-1)	502.5	55.1	0.0282	521.2	0.9978
7	125 (0)	0.25 (-1)	7 (1)	385.5	73.5	-	-	-
8	125 (0)	0.52 (0)	3 (-1)	306.7	43.3	0.0445	311.8	0.9989
9	125 (0)	0.52 (0)	5 (0)	335.6	61.0	0.0292	366.6	0.9991
10	125 (0)	0.52 (0)	7 (1)	369.8	69.0	0.0146	391.2	0.9978
11	125 (0)	0.80 (1)	3 (-1)	379.2	41.4	0.0811	385.5	0.9897
12	125 (0)	0.80 (1)	7 (1)	301.7	42.2	-	-	-
13	200 (1)	0.25 (-1)	5 (0)	250.9	41.8	-	-	-
14	200 (1)	0.52 (0)	3 (-1)	353.1	40.7	0.0133	377.5	0.9985
15	200 (1)	0.52 (0)	5 (0)	302.4	44.5	0.0100	354.4	0.9899
16	200 (1)	0.52 (0)	7 (1)	384.0	51.7	0.0045	421.7	0.9886
17	200 (1)	0.80 (1)	5 (0)	369.2	42.0	-	-	-

(removal percentage, *R%*) and coded values (X_{BH}, X_{Cinf}, X_{FR}) and the best fitted quadratic polynomial regression model was obtained as follows (equation 25):

$$R\% = -0.304\,X_{inf} + 23.387\,X_{BH} + 28.367\,X_{FR} +$$
$$0.007\,X_{C_{inf}}X_{BH} - 0.133X_{C_{inf}}X_{FR} - 7.944\,X_{BH}X_{FR} + 0.001\,X^2_{C_{inf}} \quad (25)$$
$$-1.772X^2_{BH} - 11.565X^2_{FR} + 27.693$$

MB removal by GO in the optimum levels of factors including influent concentration of 51 mg/L, bed height of 5.7 cm, and flow rate of 0.25 was predicted by the model to be 86% (q_e=459.3 mg/g).

Analysis of variance (ANOVA) was employed to investigate the adequacy and significance of the model. According to the ANOVA results (Table 7), the value of F_{cal} (98.34) was more than that of F_{tab} and *P* value was lower than 0.05 which shows the significance and suitability of quadratic model. Moreover, the normal probability of the residuals almost indicated no departures from the normality (Fig. 6). High coefficient of determination (R^2=0.992) and adjusted coefficient of determination (R_{Adj}^2=0.982) indicated the good agreement of experimental response values with model predicted values. The predicted R-squared (0.874) was also in reasonable agreement with adjusted R-squared and showed a good prediction of model.

The graphical interaction between the process parameters was presented using 3-dimensional response surface plots (Fig. 7). Fig. 7a shows the interactive effect of influent MB concentration and flow rate at a constant bed height (5 cm). As shown, the breakthrough time and removal percentage decreases by increasing the influent concentration. At lower concentrations of MB solution, due to the presence of fewer number of dye molecules and more active sites, more percentage of dye can be removed by the column and the active life of the column significantly increases. Fig. 7a also shows that the breakthrough time decreases with increasing the flow
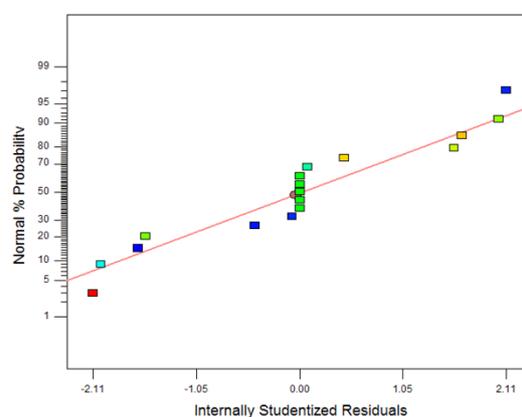
Fig. 6. Normal Probability of the Residuals in Fixed-Bed Column Optimization.

rate from 0.25 to 0.80 mL/min. This observation can be explained by this fact that more flow rate of MB solution leads to lower contact time and MB molecules will not have enough time to be adsorbed by GO particles. On the other hand, when the flow rate is increased, the removal percentage of MB is decreased.

The interaction between bed height and influent concentration at a constant flow rate (0.52 mL/min) is presented in Fig. 7b, where it is seen that as the bed height increases, due to the presence of more adsorbent amount and the increasing contact time, dye molecules have more time to contact with GO particles. Therefore, the effluent concentration of MB at the same service time in a higher bed height is lower and a larger volume and higher percentage of MB can be removed. Fig. 7c shows the interactive effect of flow rate and column bed height. This figure shows that at a constant influent concentration, the removal percentage of MB in the column increases with decreasing the flow rate and increasing the column bed height. It can be concluded that the removal percentage of MB in the fixed bed column system increases by increasing the column bed height and decreasing the

Table 7. Analysis of Variance for Response Surface Quadratic Model for the Prediction of Methylene Blue Removal Efficiency in Fixed-Bed Column System

Source	Sum of Squares (SS)	df	Mean Squares (MSS)	*F* Value	Probability (*P*) > F	
Model	2449.3	9	272.2	98.34	< 0.0001	Significant
A- Influent concentration	907.2	1	907.2	327.81	< 0.0001	Significant
B-Bed height	172.6	1	172.6	62.37	< 0.0001	Significant
C-Flow rate	972.4	1	972.4	351.37	< 0.0001	Significant
AB	3.9	1	3.9	1.41	0.2742	
AC	30.0	1	30.0	10.84	0.0133	Significant
BC	76.4	1	76.4	27.59	0.0012	Significant
A²	84.3	1	84.3	30.48	0.0009	Significant
B²	211.5	1	211.5	76.41	< 0.0001	Significant
C²	3.2	1	3.2	1.16	0.3164	
Residual	19.4	7	2.8			
Lack of fit	19.4	3	6.5	238.66	0.4	
Pure error	0.000	4	0.000			
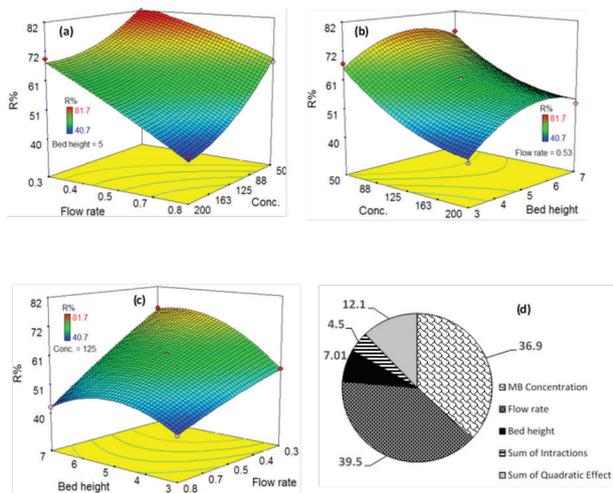
Fig. 7. 3D Response Surface Plot of the Interactive Effects of (a) pH and Adsorbent Dosage, (b) Initial Concentration and Adsorbent Dosage, (c) Initial Concentration and pH, and (d) Percentage Of Contributions (PC%) for the Possible First-Order, Quadratic and Interaction Terms Onto Adsorption Capacity (q_e) in Fixed-Bed Column System.

influent concentration and flow rate. According to Fig. 7d, flow rate and MB concentration with the contribution percepts of 39.5% and 36.9%, respectively, are the most significant terms in the fixed-bed column system. The contribution percentage for the sum of quadratic effects with 12.1%, bed height with 7.01%, and sum of interaction with 4.5% were the other important terms in the column performance.

3.4.2. Breakthrough Curve Simulated by Thomas Model

The Thomas model was fitted to the experimental data reasonably well. The kinetic coefficient (k_{Th}) and the

adsorption capacity of the column (q_{Th}) can be determined by a plot of C_{eff}/C_0 against t at various conditions using the non-linear regression method (Fig. 8a-c).

The Thomas rate constant (k_{Th}), prediction of the maximum adsorption capacity of the column (q_{Th}), and the correlation coefficient (R^2) of regression model were calculated (Table 6).

As seen in Table 6, Thomas model was able to predict the breakthrough curves very well due to its high correlation coefficient and also negligible difference between the experimental and estimated sorption capacity values. Thomas rate constant (k_{Th}) depends on the flow rate, initial MB concentration, and bed height. k_{Th} decreases by increasing the column bed height and influent concentration due to a decrease in the driving force for adsorption (20). It was also observed that the rate constant value increased from 0.0282 to 0.0811 (mL/mg min) by increasing the flow rate from 0.25 to 0.80 mL/min. However, the maximum adsorption capacity (q_{Th}) increased by increasing the bed height and decreasing the influent concentration. This is due to the fact that an increase in the initial concentration increases the competition between adsorbate molecules for the adsorption site, which ultimately results in the increased uptake rate. No clear relationship was observed between the flow rate and q_{Th}.

3.4.3. Adams–Bohart (BDST) Model and MTZ Parameters

The BDST model for different influent concentrations of MB is shown in Fig. 8a. From the slope and intercept of fitted BDST equations, the BDST parameters viz sorption rate constant (K_a) and sorption capacity (N_o) were calculated (as listed in Table 8) along with the correlation
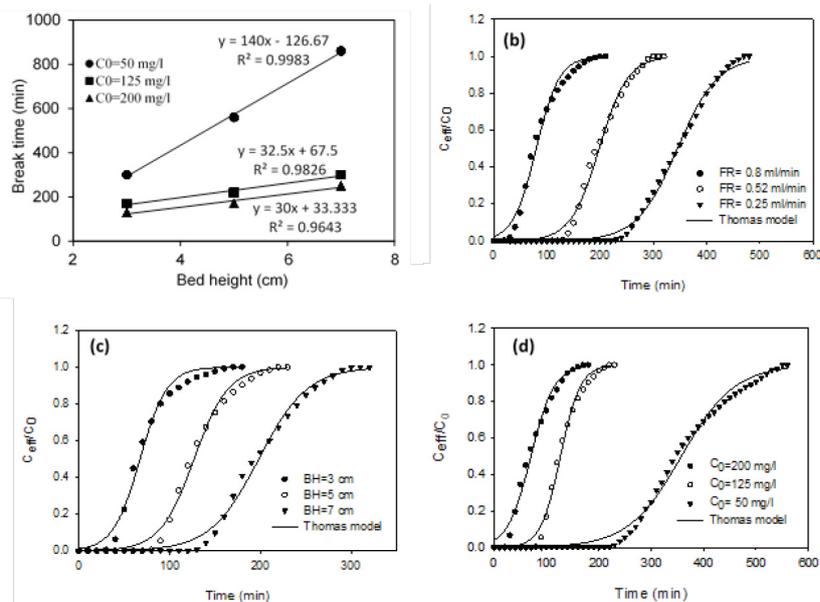
Fig. 8. BDST Graph (a) and Effects of Flow Rate (b), Bed Height (c), and Initial MB Concentration (d) in Adsorption of MB by GO on Fixed-Bed Column System.

Table 8. Bed Depth Service Time and Mass Transfer Zone Parameters for the Adsorption of MB Onto GO in Fixed-Bed Column System (at Flow Rate of 0.52 mL/min)

Runs	C_0 (mg/L)	BDST				MTZ						
		N_0 (mg/L)	K_a (L/mg min)	Z_0 (cm)	R^2	H_b (cm)	t_b (min)	t_s (min)	T_z (min)	f	Hz (cm)	Uz (cm/min)
1	50					3	135	260	125	0.71	1.68	0.013
2	50	202.2	4.82	0.010	0.998	5	265	500	235	0.75	2.67	0.011
3	50					7	430	780	350	0.70	3.63	0.010
4	125					3	45	115	70	0.68	2.27	0.032
5	125	50.6	5.39	0.041	0.993	5	95	180	85	0.76	2.67	0.031
6	125					7	150	265	115	0.74	3.42	0.030
7	200					3	20	110	90	0.37	5.09	0.057
8	200	46.9	5.61	0.044	0.953	5	35	130	95	0.52	5.60	0.059
9	200					7	85	210	125	0.72	4.99	0.040

coefficient (R^2) of the BDST model. The high values of correlation coefficient (R^2) showed that the variation of bed height with the breakthrough time was linear for all concentrations of MB. Values of rate constant, K_a, for 50, 125, and 200 mg/L influent concentrations were calculated to be 4.82, 5.39, and 5.61 mL/mg min, respectively. Rate constant shows the transfer rate of dye from the liquid phase to the solid phase. Values of rate constants are influenced by the flow rate and increase with increasing the flow rate. Since the flow rates were the same, the results showed a negligible difference between the rate constants. It can also be observed that the values of sorption capacities (N_0) of GO are decreased with the increase of influent concentration. The critical bed depths (Z_0) for 50, 125, and 200 mg/L MB concentrations were calculated to be 0.010, 0.041, and 0.044 cm, respectively, showing that critical bed depth increases with increasing the influent concentration. The reason possibly is that at more concentrations of MB, due to the presence of more dye molecules, more contact time and higher bed depth is required for the adsorption of dye molecules.

MTZ formation times (T_z) and velocities (U_z) for different influent concentrations are also shown in Table 6 at different bed depths. The results showed that by increasing the bed depth and decreasing the influent concentration, the values of T_z increased and U_z decreased. These phenomena can be attributed to the fact that diffusion process across the bed largely depends on the concentration gradient between the liquid and solid phases, and at high MB concentrations, the adsorption zone reduces due to higher diffusion flux. Further, the existence of a finite number of sorption sites, the increase of dye concentrations at a constant bed depth with time decreases the availability of active sites and reduces the throughput volume at breakthrough and exhaustion points.

4. Conclusions

The results demonstrated that GO can be used as an effective adsorbent for the removal of MB from the aqueous

solution and real wastewater in both batch and fixed-bed column adsorption system. The adsorption capacity of GO for the adsorption of MB under the optimum conditions of batch experiments (Concentration 50 mg/L; adsorbent dosage 0.05 g/L; pH 8.5) was 700 mg/g. The adsorption kinetics followed the pseudo-second order kinetic model. The results also showed that the experimental data fitted well to the Langmuir model. The endothermic nature of adsorption of MB onto GO was confirmed by the positive value of ΔH (14.95 kJ/mol). The value of the Gibbs free energy also was found to be -5.64 at 293 K, confirming the spontaneous nature of adsorption. Moreover, the breakthrough curve results showed when the bed height increases from 3 to 7 cm, the removal percentage of MB increases from 43.3% to 69%. The high value of BDST correlation coefficient also showed a good relationship between the breakthrough time and the column bed height. Furthermore, the breakthrough time decreased with increasing the flow rate from 0.25 to 0.80 mL/min and decreasing the influent MB concentration from 200 to 50 mg/L. The breakthrough curve results were fitted well to the Thomas kinetic model. Finally, parameters like critical bed depth (Z_0), movement time (T_z), MTZ height (H_z), and MTZ velocity (U_z) were calculated to characterize the MTZ and to scale up the adsorption column.

References
1. Yagub MT, Sen TK, Afroze S, Ang HM. Dye and its removal from aqueous solution by adsorption: A review. Adv Colloid Interface Sci. 2014;209:172-84. doi: 10.1016/j.cis.2014.04.002.
2. Xiao X, Zhang F, Feng Z, Deng S, Wang Y. Adsorptive removal and kinetics of methylene blue from aqueous solution using NiO/MCM-41 composite. Physica E Low

Dimens Syst Nanostruct. 2015;65:4-12. doi: 10.1016/j.physe.2014.08.006.

3. He X, Male KB, Nesterenko PN, Brabazon D, Paull B, Luong JHT. Adsorption and desorption of methylene blue on porous carbon monoliths and nanocrystalline cellulose. ACS Appl Mater Interfaces. 2013;5(17):8796-804. doi: 10.1021/am403222u.

4. Fu J, Chen Z, Wang M, Liu S, Zhang J, Zhang J, et al. Adsorption of methylene blue by a high-efficiency adsorbent (polydopamine microspheres): Kinetics, isotherm, thermodynamics and mechanism analysis. Chem Eng J. 2015;259:53-61. doi: 10.1016/j.cej.2014.07.101.

5. Sharma P, Das MR. Removal of a cationic dye from aqueous solution using graphene oxide nanosheets: investigation of adsorption parameters. J Chem Eng Data. 2013;58(1):151-8. doi: 10.1021/je301020n.

6. Robati D, Mirza B, Rajabi M, Moradi O, Tyagi I, Agarwal S, et al. Removal of hazardous dyes-BR 12 and methyl orange using graphene oxide as an adsorbent from aqueous phase. Chem Eng J. 2016;284:687-97. doi: 10.1016/j.cej.2015.08.131.

7. Mejias Carpio IE, Mangadlao JD, Nguyen HN, Advincula RC, Rodrigues DF. Graphene oxide functionalized with ethylenediamine triacetic acid for heavy metal adsorption and anti-microbial applications. Carbon. 2014;77:289-301. doi: 10.1016/j.carbon.2014.05.032.

8. Sun Y, Yang S, Chen Y, Ding C, Cheng W, Wang X. Adsorption and desorption of U(VI) on functionalized graphene oxides: a combined experimental and theoretical study. Environ Sci Technol. 2015;49(7):4255-62. doi: 10.1021/es505590j.

9. Yan H, Wu H, Li K, Wang Y, Tao X, Yang H, et al. Influence of the surface structure of graphene oxide on the adsorption of aromatic organic compounds from water. ACS Appl Mater Interfaces. 2015;7(12):6690-7. doi: 10.1021/acsami.5b00053.

10. Wang J, Chen Z, Chen B. Adsorption of polycyclic aromatic hydrocarbons by graphene and graphene oxide nanosheets. Environ Sci Technol. 2014;48(9):4817-25. doi: 10.1021/es405227u.

11. Hummers WS Jr, Offeman RE. Preparation of graphitic oxide. J Am Chem Soc. 1958;80(6):1339-. doi: 10.1021/ja01539a017.

12. Hameed BH, Tan IA, Ahmad AL. Optimization of basic dye removal by oil palm fibre-based activated carbon using response surface methodology. J Hazard Mater. 2008;158(2-3):324-32. doi: 10.1016/j.jhazmat.2008.01.088.

13. Ho YS. Citation review of Lagergren kinetic rate equation on adsorption reactions. Scientometrics. 2004;59(1):171-7. doi: 10.1023/B:SCIE.0000013305.99473.cf.

14. Ho YS, McKay G. Pseudo-second order model for sorption processes. Process Biochem. 1999;34(5):451-65. doi: 10.1016/S0032-9592(98)00112-5.

15. Weber WJ , Morris JC. Kinetics of adsorption on carbon from solution. J Sanit Eng Div Proc Am Soc Civ Eng. 1963;89(2):31-60.

16. Langmuir I. The constitution and fundamental properties of solids and liquids. Part I. Solids. J Am Chem Soc. 1916;38(11):2221-95. doi: 10.1021/ja02268a002.

17. Freundlich H. Over the adsorption in solution. J Phys Chem. 1906;57:385-470.

18. Chabani M, Amrane A, Bensmaili A. Kinetic modelling of the adsorption of nitrates by ion exchange resin. Chem Eng J. 2006;125(2):111-7. doi: 10.1016/j.cej.2006.08.014.

19. Ding Z, Hu X, Morales VL, Gao B. Filtration and transport of heavy metals in graphene oxide enabled sand columns. Chem Eng J. 2014;257:248-52. doi: 10.1016/j.cej.2014.07.034.

20. Shahbazi A, Younesi H, Badiei A. Functionalized SBA-15 mesoporous silica by melamine-based dendrimer amines for adsorptive characteristics of Pb (II), Cu (II) and Cd (II) heavy metal ions in batch and fixed bed column. Chem Eng J. 2011;168(2):505-18. doi: 10.1016/j.cej.2010.11.053.

21. Han R, Ding D, Xu Y, Zou W, Wang Y, Li Y, et al. Use of rice husk for the adsorption of congo red from aqueous solution in column mode. Bioresour Technol. 2008;99(8):2938-46. doi: 10.1016/j.biortech.2007.06.027.

22. Hasan SH, Ranjan D, Talat M. Agro-industrial waste 'wheat bran' for the biosorptive remediation of selenium through continuous up-flow fixed-bed column. J Hazard Mater. 2010;181(1-3):1134-42. doi: 10.1016/j.jhazmat.2010.05.133.

23. Aksu Z, Gonen F. Biosorption of phenol by immobilized activated sludge in a continuous packed bed: prediction of breakthrough curves. Process Biochem. 2004;39(5):599-613. doi: 10.1016/S0032-9592(03)00132-8.

24. Debnath S, Maity A, Pillay K. Impact of process parameters on removal of Congo red by graphene oxide from aqueous solution. J Environ Chem Eng. 2014;2(1):260-72. doi: 10.1016/j.jece.2013.12.018.

25. Shen J, Hu Y, Shi M, Lu X, Qin C, Li C, et al. Fast and facile preparation of graphene oxide and reduced graphene oxide nanoplatelets. Chem Mater. 2009;21(15):3514-20. doi: 10.1021/cm901247t.

26. Tan P, Sun J, Hu Y, Fang Z, Bi Q, Chen Y, et al. Adsorption of Cu2+, Cd2+ and Ni2+ from aqueous single metal solutions on graphene oxide membranes. J Hazard Mater. 2015;297:251-60. doi: 10.1016/j.jhazmat.2015.04.068.

27. Zhang F, Wang B, He S, Man R. Preparation of graphene-oxide/polyamidoamine dendrimers and their adsorption properties toward some heavy metal ions. J Chem Eng Data. 2014;59(5):1719-26. doi: 10.1021/je500219e.

28. Hameed BH, Din AT, Ahmad AL. Adsorption of methylene blue onto bamboo-based activated carbon: kinetics and equilibrium studies. J Hazard Mater. 2007;141(3):819-25. doi: 10.1016/j.jhazmat.2006.07.049.

29. Chowdhury S, Mishra R, Saha P, Kushwaha P. Adsorption thermodynamics, kinetics and isosteric heat of adsorption of malachite green onto chemically modified rice husk. Desalination. 2011;265(1-3):159-68. doi: 10.1016/j.desal.2010.07.047.

30. Li Y, Sun J, Du Q, Zhang L, Yang X, Wu S, et al. Mechanical and dye adsorption properties of graphene oxide/chitosan composite fibers prepared by wet spinning. Carbohydr Polym. 2014;102:755-61. doi: 10.1016/j.carbpol.2013.10.094.

31. Shahbazi A, Bagheri Zonoz F. Decolorization of Malachite green dye from wastewater by Populus deltoides: three-level Box–Behnken design optimization, equilibrium, and kinetic studies. J Water Reuse Desalin. 2015;5(3):250-63. doi: 10.2166/wrd.2015.085.

32. Juang RS, Wu FC, Tseng RL. Mechanism of Adsorption of Dyes and Phenols from Water Using Activated Carbons Prepared from Plum Kernels. J Colloid Interface Sci. 2000;227(2):437-44. doi: 10.1006/jcis.2000.6912.

33. Kannan N, Sundaram MM. Kinetics and mechanism of removal of methylene blue by adsorption on various carbons—a comparative study. Dyes Pigm. 2001;51(1):25-40. doi: 10.1016/S0143-7208(01)00056-0.

34. Vijayaraghavan K, Padmesh TV, Palanivelu K, Velan M. Biosorption of nickel(II) ions onto Sargassum wightii: application of two-parameter and three-parameter isotherm models. J Hazard Mater. 2006;133(1-3):304-8. doi: 10.1016/j.jhazmat.2005.10.016.

35. Foo KY, Hameed BH. Insights into the modeling of adsorption isotherm systems. Chem Eng J. 2010;156(1):2-10. doi: 10.1016/j.cej.2009.09.013.

36. Mahmoud DK, Mohd Salleh MA, Ab Karim Ghani WA, Idris A, Abidin ZZ. Batch adsorption of basic dye using acid treated kenaf fibre char: Equilibrium, kinetic and thermodynamic studies. Chem Eng J. 2012;181-182:449-57. doi: 10.1016/j.cej.2011.11.116.